Anomalous temperature behavior of Sn impurities

D. Haskel and H. Shechter
Department of Physics, Technion, Haifa, Israel

E. A. Stern and M. Newville
Department of Physics FM-15, University of Washington, Seattle, Washington 98195

Y. Yacoby
Racah Institute of Physics, Hebrew University, Jerusalem, Israel
(Received 26 May 1992)

Sn impurities in Pb and Ag hosts have been investigated by Mössbauer effect and in Pb by x-ray-absorption fine-structure (XAFS) studies. The Sn atoms are dissolved up to at least 2 at. % in Pb and up to at least 8 at. % in Ag for the temperature ranges investigated. The concentration limit for Sn-Sn interactions is 1 at. % for Pb and 2 at. % for Ag as determined experimentally by lowering the Sn concentration until no appreciable change occurs in the Mössbauer effect. XAFS measurements verify that the Sn impurities in Pb are dissolved and predominantly at substitutional sites. For both hosts the temperature dependence of the spectral intensities of isolated Sn impurities below a temperature T_0 is as expected for vibrating about a lattice site. Above T_0 the Mössbauer spectral intensity exhibits a greatly increased rate of drop-off with temperature without appreciable broadening. This drop-off is too steep to be explained by ordinary anharmonic effects and can be explained by a liquidlike rapid hopping of the Sn, localized about a lattice site. Higher-entropy-density regions of radii somewhat more than an atomic spacing surround such impurities, and can act as nucleation sites for three-dimensional melting.

I. INTRODUCTION

The bulk melting of solids is well understood thermodynamically. However, thermodynamics, being a macroscopic theory, does not reveal the microscopic behavior or the mechanism of the melting transition, i.e., how the liquid nucleates at the melting point. A first-order phase transition like melting cannot transform continuously from the solid to the liquid but must do so discontinuously. It is expected that melting will be an inhomogeneous nucleation process where the nucleation starts about particular sites and grows to encompass the whole sample. Molecular-dynamic simulations[1] have shown that grain boundaries and surfaces can act as nucleation sites in agreement with experiments.[2–4] However, in the thermodynamic limit where the sample dimensions become extremely large the effects of such boundaries must become negligible and a nucleation site that scales with the volume is required. The most likely fluctuations that can lead to nucleation sites are those that are short ranged (of the order of interatomic distances). These scale correctly with the volume. We have found experimental evidence[5,6] that around some impurities there exists already below the melting point a somewhat more disordered region which one expects would have a smaller barrier to fluctuate to a nucleation site than the undisturbed bulk.

To experimentally investigate such nucleation sites of melting requires a short-ranged probe. Thus, diffraction techniques which are mostly sensitive to long-range order are not the best probes to investigate the nucleation mechanism. The short-range probes that we employed to investigate the nucleation of melting mechanisms were Mössbauer effect (ME) (Ref. 5) and the x-ray-absorption fine-structure technique (XAFS).[6] The criterion usually used by physicists to distinguish between a solid and its liquid is the presence of long-range order in the former and its disappearance in the latter. The short-range probes are not sensitive to long-range order and a different criterion must be employed to distinguish between a solid and a liquid for these techniques. Macroscopically, the most obvious difference between a solid and its liquid is the response under shear stresses. Liquids have no resistance to static shears, and, at the melting point where they coexist, the viscosity of the liquid is many orders of magnitude less than the solid. By the Stokes-Einstein relation this difference in viscosity is due to a typically 10^5 increase in the diffusion rate in the liquid relative to the solid. A second striking macroscopic difference is the increased entropy in the liquid as revealed by the latent heat of melting.

Both these features can be detected by a local probe. In the case of the ME the increased hopping rate of the liquid is typically so great that the spectral intensity becomes negligible. In the case of XAFS, as shown for liquid Pb,[7] the increased hopping rate decreases the signal by the fraction of the time an atom is hopping from the site about which it vibrates. In liquid Pb, an atom spends about a half of its time vibrating and the rest diffusing.[7] The mechanism of diffusion in a liquid is quite different than in a solid because it is a high entropy process involving many atoms flowing around the diffusing atom resulting in the 10^5 increase in its rate. The local probe can distinguish a liquidlike region by either detecting an enhanced hopping and/or an increased entropy

0163-1829/93/47(21)/14032(12)/$06.00

density.

In the case of a 1 at. % Sn alloy in Pb, the ME showed[5] that the spectral intensity of the Sn atoms drops precipitously at around 150 K, about $\frac{1}{4}$ of the melting temperature. This rapid drop is too steep to be explained by anharmonicity of the vibration of the Sn atoms. It is caused by an anomalously rapid hopping of the Sn atoms about a lattice site within a "bubble" containing a large entropy density involving a coherent motion of ~20–40 surrounding atoms. XAFS measurements[6] also indicated premelting phenomena about the Hg atoms in a 4 at. % alloy of Hg in Pb starting around 400 K. Again an anomalously rapid hopping of the Hg atoms localized about its original lattice site is indicated by these measurements.

In this paper we will present more detailed measurements in these systems which will relate to concerns expressed by Mullen,[8] and Martin and Singer[9] about the original interpretation of the results. We also present some results on impurities in a Ag host to ascertain the generality of the results observed in the Pb host. The outline of the paper is as follows. Section II gives the experimental results. A discussion and interpretation of the experiments are given in Sec. III. A summary and conclusion are given in Sec. IV.

II. EXPERIMENTAL TECHNIQUES AND RESULTS

A. Sample preparation

The samples were made from 99.999% pure host (Pb or Ag) and either Sn enriched to 84% ^{119}Sn isotope or natural Sn (which contain ~8% ^{119}Sn). The components used were all in the form of small pellets except for the ^{119}Sn, which was in powder form and had been reduced from a powder of enriched SnO_2. This reduction was done under a H_2 atmosphere at 1200 K for 1 h.

The correct mixture of components were weighed to a total mass between 2.5 and 10 g and put in a quartz ampule which was then evacuated by a mechanical pump and sealed. In order to assure that the two component elements would mix well, the samples were then heated over a flame until the Sn melted (the Pb host, when used, was also melted) and mechanically shaken. The samples were held in a furnace at least 50 K above the melting temperature of the pure host for 24 h, and then quenched into cold water. After inspecting the ampule to determine that it had not cracked during the heating or quenching, the ingot was extracted and cold rolled into a foil. The final thickness of the foil was determined so that the sample would be about 1 absorption thickness for nonresonant 24 keV x rays. This foil was coated with a thin film (~1000 Å) of aluminum to inhibit oxidation. For the samples with a Ag host, this Al film itself was oxidized by suspending over boiling water to prevent the Al from diffusing into the Ag host. The aluminum coating did not need to be oxidized for the Pb host alloys because Al does not dissolve in Pb.

Alloys with various compositions were made in this way. For the Pb host, the samples used had enriched Sn concentrations of 0.5, 1.0, 2.0, 3.0, and 5.0 at. % (the room-temperature solubility limit for Sn in Pb is ~3 at. %). For the Ag host, the samples used had enriched Sn concentrations of 1.0, 2.0, 4.0, and 8.0 at. % and natural Sn concentration of 4 at. % (the solubility limit for Sn in Ag is ~12 at. %). The relative Sn concentrations of the alloys were confirmed by XAFS, Auger depth analysis, and EDS (energy dispersive spectroscopy). XAFS measurements determined that the relative Sn abundance for the 1.0, 2.0, and 5.0 at. % Sn-Pb had the ratio 1:2:5. Auger depth analysis gave the ratio for 1, 2, and 4 at. % Sn-Ag as 1:(1.6):(4.7). EDS gave the ratio for 1, 2, and 4 at. % Sn-Ag as 1:(2.1):(3.2).

B. Spectroscopy

The Mössbauer measurements were performed with the alloys as the fixed absorber versus a moving gamma source in a constant acceleration mode. The source was ^{119}Sn in a calcium stannate ($CaSnO_3$) matrix with linewidth $\Gamma_s = 0.382$ mm/s. The velocity scale was determined from the quadrupole splitting[10] of SnF_2.

The Pb-Sn alloys were cooled by a flow of liquid nitrogen through a cold finger. The temperature was controlled by a microprocessor within 0.05%. The Ag:Sn samples were heated to desired temperatures and kept stable within 0.5%. It was important to keep the temperature (T) constant for the long run time at each T (up to 3 days) for better statistics caused by the weak intensity that prevailed at high temperatures due to the low Mössbauer fraction coupled with the low isotope content in the sample. To check the apparatus, a 0.1-mm-thick sample of natural metallic tin supplied by the source manufacturer (Amersham International) was measured at 80 K. The on-resonance dip was as expected from the estimated Mössbauer fractions.

Figure 1 shows a typical set of spectra obtained from Ag 4 at. % Sn at different T's. Figure 2 shows the corresponding information for a Pb 1 at. % Sn sample. Note that the relative decrease in spectral intensity for Pb 1 at. % Sn is much greater between 145 and 150 K than that between 140 and 145 K. The solid curve through the data points is a result of a Lorentzian best fit using a standard commercial software package. The analyses yield the spectral intensity, line position (shift), and width. The spectral intensity I is the integrated area of the data after subtraction of the background. Attempts to fit more than one Lorentzian resulted in poorer fits.

In order to evaluate the effect of the absorber thickness,[11] we plotted experimental linewidth Γ versus absorber effective thickness at room temperature for the Ag alloys. Γ initially increases linearly with thickness and starts to saturate at large thicknesses. Extrapolation to zero thickness results in an experimental linewidth Γ of ~0.82 mm/s. The absorber linewidth is 0.44 mm/s (=0.82–0.38 mm/s of the source), as compared to the natural linewidth of the 24 keV isomer level of 0.32 mm/s. The "zero thickness" broadening could result from local inhomogeneities of electric-field gradients induced by the long-range Friedel oscillations of the shielding tails around the tin impurities causing quadrupole

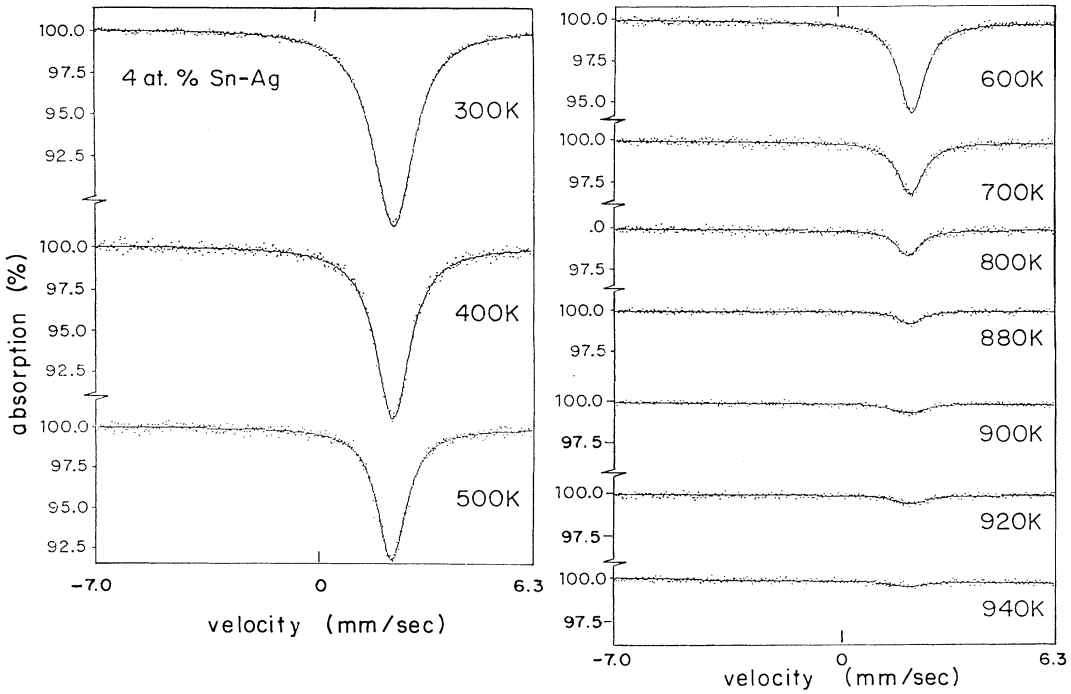

FIG. 1. Mössbauer spectra for a 4 at. % Sn in Ag alloy at the various indicated temperatures. The solid line is the Lorentzian fit used to obtain the various parameters utilized in the interpretation of the data.

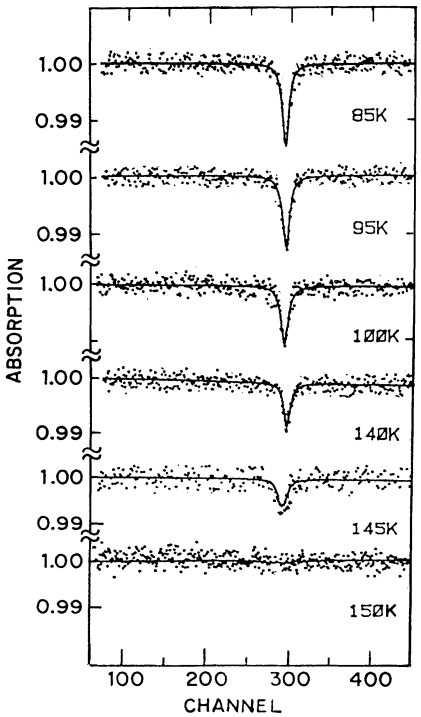

FIG. 2. Mössbauer spectra for a 1 at. % Sn in Pb alloy at the various indicated temperatures. The solid line is the Lorentzian fit used to obtain the various parameters utilized in the interpretation of the data.

splitting.[12] This interpretation is consistent with the larger high-temperature width for the Ag matrix than the Pb one. The tails will be much weaker for the Pb matrix which has the same valence charge as the Sn.

Concomitant with line broadening, excess absorber thickness decreases the spectral intensity I as checked by comparing the two Ag alloys of 4% natural Sn and 4% enriched Sn (Fig. 3). For the same sample thickness the enriched sample has about 10 times the resonance absorption as the natural sample. As the temperature increased above room temperature the enriched sample varied from a thick to a thin resonance absorber because of the decreased Mössbauer fraction. At room temperature the enriched sample has a $t_a \sim 6$, where t_a is the effective absorber thickness at its resonance peak,[13] while thin absorbers satisfy the relation $t_a \leq 1$. The natural sample remained thin throughout this temperature range as shown by its linewidth in Fig. 3(b). Lining up the $\ln I$ versus T plots at high temperature, as is done in Fig. 3(a), the enriched sample plot falls below the natural sample as room temperature is approached. To avoid any spurious variations introduced by this decrease of the spectral intensity as the resonance thickness increases, the data were analyzed only in the "thin" range as monitored by the linewidth, where saturation effects were negligible.

C. Results

The temperature dependence of the spectral intensity for Ag alloys is shown in Fig. 3(a) for thin absorbers, and

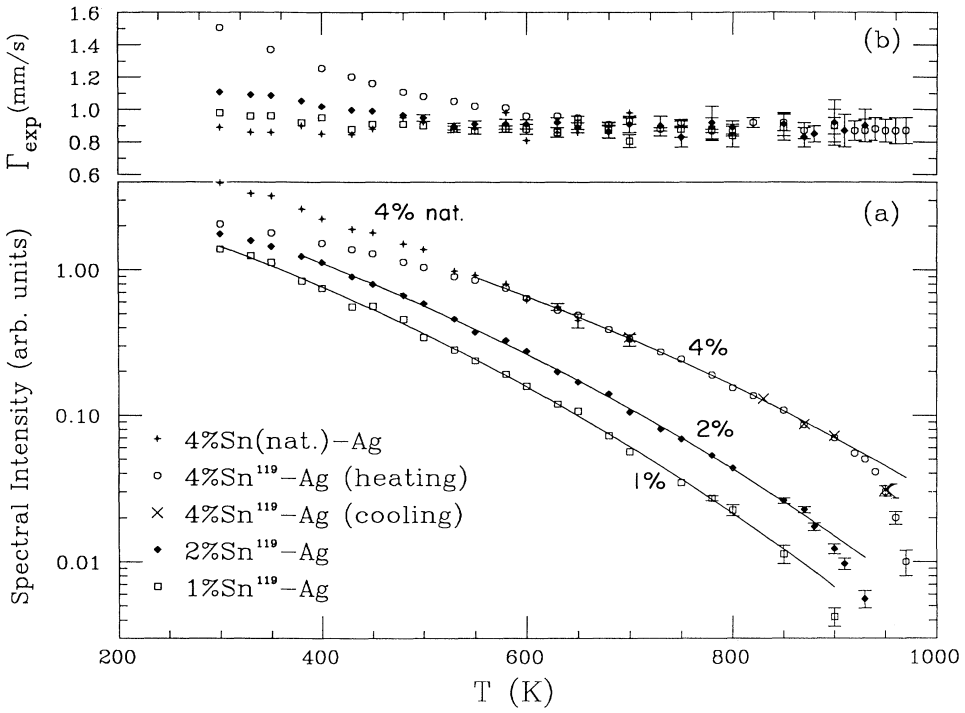

FIG. 3. (a) Plots of ln$I$ vs T for alloys with 1, 2, and 4 at. % Sn (all enriched) and 4 at. % natural Sn in Ag, not corrected for saturation effects. Unless shown, error bars are the same size or smaller than the symbol used. ×'s show data collected during cooling, while the rest of the points are on heating. The solid lines are fits to experimental data using an anharmonic model. (b) Plots of linewidth Γ vs T for the same alloys.

for Pb alloys in Fig. 4(a). To increase clarity, each curve has been moved vertically by an arbitrary amount. Since several factors, such as sample thickness and Sn concentration, also add a constant to the ln$I$ even when the effect per atom is a constant, we limit out measurements to the temperature dependence of the spectral intensity, and ignore the offset value. The ln$I$ varies linearly with T at low temperatures as expected for harmonic vibrations.[14] As the temperature increases for the Ag hosts a gradual deviation from linear variation sets in and at above 900 K a more rapid drop occurs. There is a weak concentration dependence in the temperature dependence of the samples. The Pb hosted alloys show a more spectacular concentration and temperature dependence. As the concentration increases the anomalous drop from the linear Debye-Waller behavior becomes less precipitous,

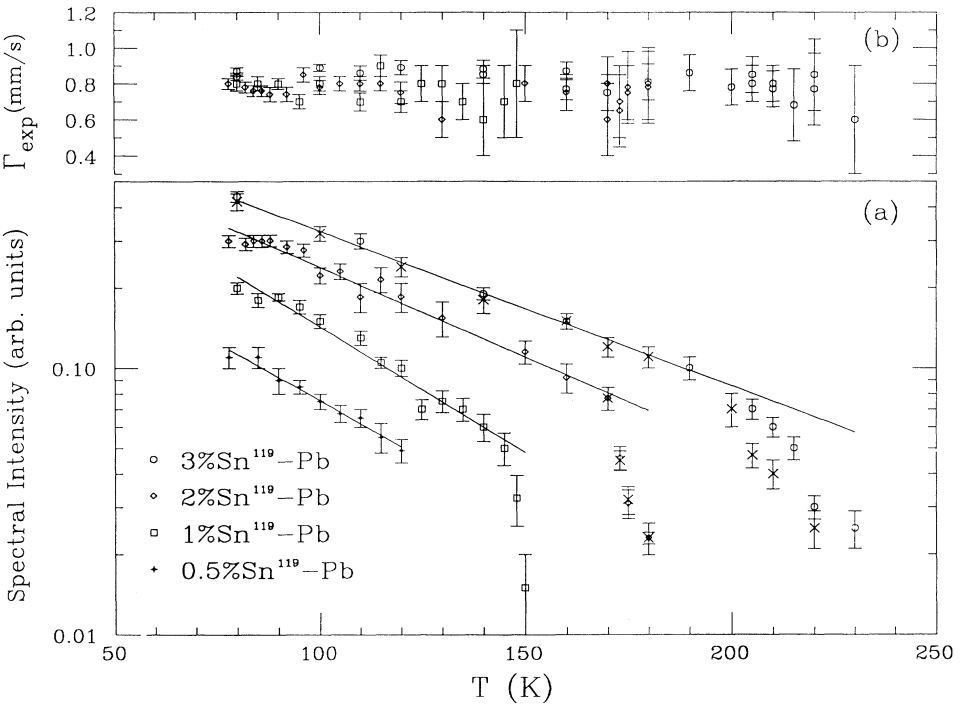

FIG. 4. (a) Plots of ln$I$ vs T for alloys with 0.5, 1, 2, and 3 at. % Sn (all enriched) in Pb. ×'s show data collected during cooling, while the rest of the points are on heating. Unless shown, error bars are the same size or smaller than the symbol used. The solid lines are fits to a harmonic model. The highest temperature point of the 1 at. % Sn curve has an asymmetrical error bar with a lower limit near zero. (b) Plots of linewidth Γ vs T for the same alloys.

TABLE I. Thermodynamic properties of "premelted" bubbles. $\ln I = \ln I_0 + \alpha T + \beta T^2$. E and S are, respectively, the energy and entropy differences between the vibrating state 1 and the excited state 2. L is an estimate of the number of surrounding atoms participating in the impurity hopping in the excited state 2.

Host	% Sn	α (10^{-3} K^{-1})	β (10^{-6} K^{-2})	E (eV)	S (k_B)	L
Pb	0.5	−20(2)				
Pb	1	−22(2)		0.4	30	30
Pb	2	−14(2)		0.7	40	40
Ag	2	−2.3(0.3)	−3.1(0.3)	3.3	40	35
Ag	4	−2.6(0.3)	−3.3(0.2)	6.1	70	62

and occurs at a higher temperature. The 3% sample is near the solubility limit at room temperature, and reversibility checks discussed below show some precipitation at lower temperatures. The 2%, 1%, and $\frac{1}{2}$% samples are fully dissolved at low temperatures and yet there is a significant difference between the 2% and the other two samples. Both the linear slope and the rapid drop are different. The intensity of the $\frac{1}{2}$% sample was too small to follow up to the temperature T_0 where the rapid drop occurs. However, since the $\frac{1}{2}$% sample has the same slope as the 1% sample, as listed in Table I, we assume that its full temperature dependence is the same and infer that interactions between impurities have a negligible effect on the Mössbauer effect for concentrations of 1% and less. We will discuss the deviations from linearity for the isolated impurities in the next section but we did an experimental check to verify that the rapid decrease in intensity was not due to the onset of a broadened line due to, say, bulk diffusion. To further test the assumption of only one unbroadened Lorentzian in the Pb 1 at. % Sn data, the background was determined by fitting the shoulders of the spectra, away from the drop, with a straight line and determining the total area below this line by adding all the points. The resulting area agreed with the best fit of a single Lorentzian for all spectra within the uncertainties of the fits.

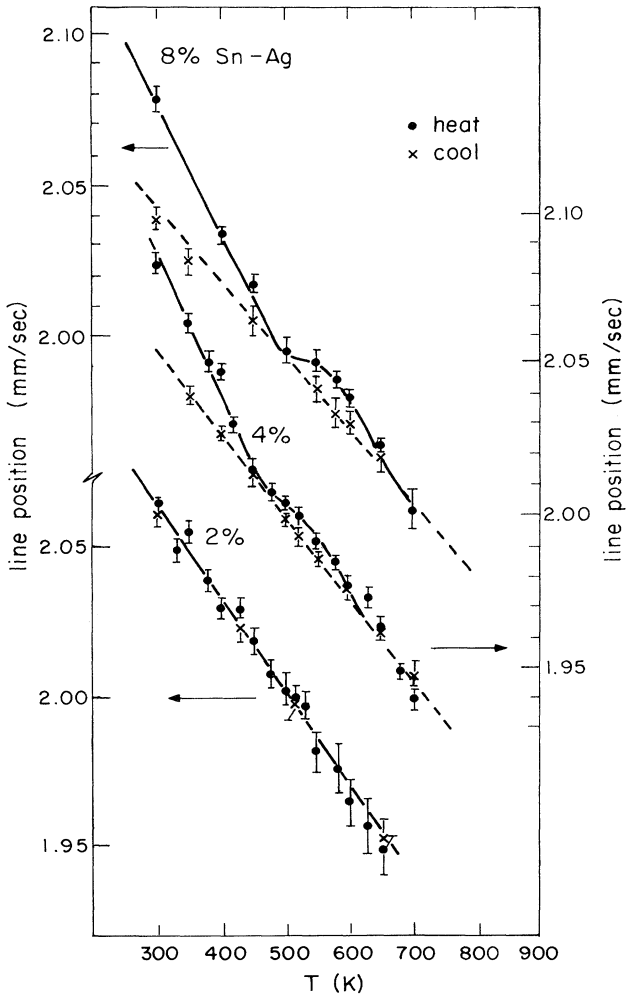

FIG. 5. Plot of line shift vs T for 2, 4, and 8 at. % Sn (enriched) in Ag alloys. The dots are during heating and the ×'s are during cooling. The vertical scale is displaced downward by 0.05 and 0.10 for the 4 and 2% samples, respectively. The line is a guide to the eye.

Figures 3(b) and 4(b) display the linewidth Γ vs T dependence for Ag and Pb based alloys, respectively. The line shifts are shown versus T in Figs. 5 and 6 for the Ag and Pb based alloys, respectively. Both the linewidths and line shifts have the expected behavior for the Pb hosts. However, the line shifts for 4% and 8% Ag samples have a shift from a linear temperature dependence which does not occur for the 2% sample. From the disappearance of the shift at low concentration we infer that the isolated impurity behavior is linear.

We checked the reversibility of the Mössbauer signal for the 2 and 3 at. % Sn in Pb samples and for the 2, 4, and 8 at. % Sn in Ag samples. Measurements were performed as the samples were heated and cooled. The results for $\ln I$ are shown in Fig. 3(a) for the Ag alloys and in 4(a) for the Pb alloys, while the line shifts of the Ag alloys are shown in Fig. 5. The Pb alloy line shifts were verified to be reversible for the 2 at. % sample. The ×'s in Figs. 3(a) and 4(b) are on cooling and the rest of the points are on heating. The solid dots in Fig. 5 show the results for the Ag alloys on heating while the ×'s are on cooling. The 3% Pb sample was the only one that showed appreciable irreversibility in its $\ln I$. The 4% and 8% Ag samples displayed irreversibility in line shift on the initial cycle. The 4% sample was cycled a second

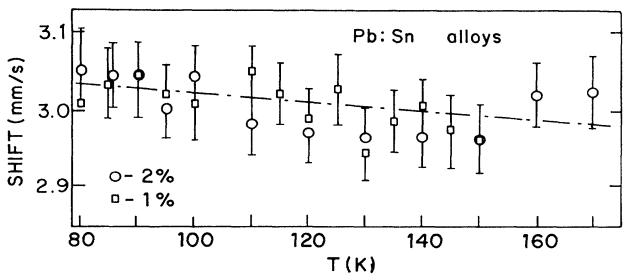

FIG. 6. Plot of line shift vs T for 1 and 2 at. % Sn in Pb alloys. The line is a guide to the eye.

time and the irreversibility disappeared. The significance of these results are discussed in the next section.

III. DISCUSSION

The Mössbauer spectral intensity is proportional to the recoilless fraction of the Mössbauer signal.[15] We distinguish two mechanisms that decouple the Mössbauer nucleus from the lattice and decrease the recoilless fraction. One is the nucleus vibrating about a given site in the lattice and the other is the nucleus hopping away from the lattice site.

Vibrations decrease the recoilless fraction[15] by a Debye-Waller factor $e^{-q^2\sigma^2}$ where, expanding in the anharmonic potential

$$V(x)=\tfrac{1}{2}kx^2+ax^3+bx^4 , \tag{1}$$

$$\sigma^2=\left[\frac{k_BT}{k}+12\left[\frac{k_BT}{k}\right]^2\frac{1}{k}\left[\frac{3a^2}{k}-b\right]\right]+\mathcal{O}(T^3) . \tag{2}$$

Here k_B is the Boltzmann constant, q is the Mössbauer gamma-ray wave number ($q\simeq 12.1$ Å^{-1} for ^{119}Sn), and σ^2 is the mean-squared vibration amplitude, $\sigma^2=\langle(\hat{\mathbf{q}}\cdot\mathbf{u})^2\rangle$. The result is valid in the classical limit $k_BT\gg\hbar\omega_0$, where ω_0 is the highest frequency of the solid. Terms which contribute proportional to T^3 and higher powers are neglected.

The simple one-dimensional potential of Eq. (1) is equivalent to an Einstein model for the vibrational motion of the Mössbauer atom. This crude model is sufficient to parameterize correctly the temperature dependence of σ^2 in the classical limit as given in Eq. (2). A more exact theory valid in the quantum limit also, though only in the harmonic approximation, has been presented by Mannheim[16] and has been used by Howard and Nussbaum[17] to analyze the behavior of Fe impurities in various hosts.

As seen in greater detail further down, the decrease of $\ln I$ with temperature below T_0 is almost linear and can be fully accounted for by the anharmonic model. However, this mechanism, even with a T^3 term, cannot account for the rapid drop in intensity above T_0 in either Pb or Ag. To explain this behavior we propose a locally correlated hopping model. The hopping will not contribute to bulk diffusion if the hopping atom remains localized about a particular lattice site. In this sense the hopping is highly correlated. Whereas the onset of bulk diffusion replaces the recoilless line with a broadened one, localized hopping does not entirely eliminate the recoilless fraction.

In our model the Mössbauer atom has two possible states. State 1, with probability P, corresponds to the atom vibrating about the initial site with a mean-squared disorder σ_1^2 as given by Eq. (2). State 2, with probability $(1-P)$, corresponds to the atom hopping from the initial site with a mean-squared displacement of σ_2^2. The Mössbauer spectrum for this model is given by

$$W(q,\omega)=Pe^{-q^2\sigma_1^2}[P\mathcal{L}(\Gamma,\omega)+(1-P)\mathcal{L}(\Gamma+\Delta,\omega)]+2P(1-P)e^{-(q^2/2)(\sigma_1^2+\sigma_2^2)}[\mathcal{L}(\Gamma,\omega)-\mathcal{L}(\Gamma+\Delta,\omega)]$$
$$+(1-P)e^{-q^2\sigma_2^2}[(1-P)\mathcal{L}(\Gamma,\omega)+P\mathcal{L}(\Gamma+\Delta,\omega)] , \tag{3}$$

where $\mathcal{L}(\Gamma,\omega)$ is a Lorentzian

$$\mathcal{L}(\Gamma,\omega)=\frac{1}{\pi}\frac{(\Gamma/\hbar)}{(\omega)^2+(\Gamma/\hbar)^2} \tag{4}$$

and $\Delta/\hbar$ is the decay rate from state 1 (taken as the initial state) to an equilibrium distribution of states 1 and 2. Equation (3) is derived in the Appendix. The Mössbauer spectral intensity is given by

$$I=\int W(q,\omega)d\omega , \tag{5}$$

where the integration is done only over the sharp line, so that any significant broadening contributes to the background.

Making the assumption that the states are in thermal equilibrium at all temperatures, the relative occupation probability is given by

$$\frac{P}{1-P}=\frac{e^{-E_1/k_BT}}{g_2e^{-E_2/k_BT}}=\frac{e^{E/k_BT}}{g_2} , \tag{6}$$

where E is the energy difference between the states and g_2 is the degeneracy of the high-energy state relative to that of the low-energy state. To estimate the degeneracy g_2 we assume that, whereas one atom is involved in the low-energy state, L atoms are involved in the hopping process and $g_2\approx n^L$ corresponding to typically n states per atom. For a rough estimate we assume $n=2$. Defining a local configurational entropy

$$S=k_B\ln g_2\approx Lk_B\ln 2 , \tag{7}$$

Eq. (6) becomes

$$\frac{P}{1-P}=e^{(E-TS)/k_BT} . \tag{8}$$

We note from Eq. (3) that Δ broadens the Mössbauer linewidth. For cases in which there is no significant line broadening, either (a) $\Delta\ll\Gamma$ or (b) $\Delta\gg\Gamma$. Since the high-energy state does not contribute to the Mössbauer spectra intensity we know that $q^2\sigma_2^2\geq 5$. For the Sn Mössbauer line with $q\simeq 12.1$ Å^{-1}, it is required to have $\sigma_2>0.2$ Å to satisfy this assumption. In case (a) Eqs. (5) and (6) give

$$I=Pe^{-q^2\sigma_1^2} , \tag{9a}$$

while in case (b) they give

$$I=P^2e^{-q^2\sigma_1^2} . \tag{9b}$$

Because XAFS has a different measurement time scale than ME, it can distinguish between the two cases (a) and (b) that the Mössbauer measurements allow. The Mössbauer lifetime is $\sim 10^{-7}$ s while the XAFS measurement time is $\sim 10^{-15}$ s, so that Mössbauer measurements average over many lattice vibrations ($\omega_0^{-1} \simeq 10^{-13}$ s) for each atom, while XAFS measures an essentially instantaneous average distribution of atoms.

In case (a) the nucleus does not exchange its state during the Mössbauer lifetime. Both ME and XAFS see an essentially instantaneous average of the atomic distribution with a fraction P in the low-energy state and $(1-P)$ in the high-energy state, and neither technique sees many transitions between these states. The σ^2 from XAFS would show the same qualitative behavior as the ME σ^2 in this case. Although XAFS and Mössbauer measure different σ^2 (Mössbauer measures the σ^2 relative to a lattice site and XAFS the σ^2 relative to its neighbors) the relative size of the σ^2 should be similar. In order for case (a) to have the Mössbauer spectral intensity decrease dramatically above T_0, the high-energy state must have a $\sigma_2^2 \gg \sigma_1^2$. Thus, for case (a), as the temperature is varied through T_0 the σ^2 measured by XAFS should also change abruptly from σ_1^2 to a much larger σ_2^2.

In case (b) the nucleus makes many transitions between the two states during the Mössbauer lifetime, but does not make transitions between the two states during the XAFS time, and it is possible for the σ^2 of XAFS and Mössbauer to be quite different above T_0. Since the nucleus is making many hopping transitions during the Mössbauer lifetime, the σ from ME would be determined by the hopping length $\simeq \sigma_2$. However, the hopping time could be short compared to the time between hops, when the nucleus is vibrating about a particular site with a mean-square disorder σ_1^2. The XAFS σ^2 would still be $\simeq \sigma_1^2$, and the XAFS signal would be only slightly decreased by the fraction of the time spent hopping, as seen in XAFS measurements on liquid Pb. XAFS measurements on a 2% Sn in Pb sample show no significant change in σ^2 around T_0 besides the ordinary Debye-Waller dependence. This behavior rules out case (a), and case (b) is the one that applies to Pb:Sn alloys.

We consider another possible interpretation of the dramatic decrease in Mössbauer intensity, suggested by Mullen,[8] that the impurity does not remain dissolved at all temperatures but partially precipitates out as the temperature is lowered or raised. The decrease in Mössbauer spectral intensity is caused by the precipitated particles having a smaller force constant k and consequent larger σ^2 as given by Eq. (2). The phase diagram[18] does show a decreasing solubility limit with temperature near room temperature which, if extrapolated, may cross the 2% and even 1% limits at low enough temperatures. This possibility can be ruled improbable by the low temperatures of 150 K where the putative precipitation would occur. At such low temperatures the possibility of any coalescence of the impurities into a precipitate would be improbable because of the absence of bulk diffusion or grain boundary movement. The large decrease would require a sudden precipitation of most of the impurities which means that the solubility must decrease to a value well below 1%. Any reasonable extrapolation of the solubility limits would not be consistent with such a low value.

Three measurements we performed show clearly that precipitation does not occur. The first is to measure any hysteresis in the temperature dependence of the rapid decrease near T_0. As shown in Fig. 4(a) there is no hysteresis found for the Mössbauer spectral intensity for the 2% Sn in Pb sample. A hysteresis was found for the 3% sample in Pb which is above the solubility limit ($\sim 2\%$) at room temperature and may be expected to have some further precipitation at lower temperatures. For comparison, in an investigation of the precipitation of Sn in Pb, the spectral intensity for an 8 at. % Sn in Pb sample was measured by Arriola and Cranshaw[19] up to 520 K. They found that the spectral intensity had a hysteresis effect in the temperature range of 320–360 K, as precipitation occurred. Above 360 K the Sn is completely dissolved, and a Θ_D of 104 K was found. This value is consistent with our value of 107 K determined at low temperatures for the 2% and 3% samples. Extrapolating the results of Arriola and Cranshaw above 320 K to 80 K, assuming that $\Theta_D = 104$ K, we find that their spectral intensity is about 8 times that of ours, as shown in Fig. 2, in agreement with the ratio of concentrations. Our 2% Sn-Pb sample did not show the hysteresis expected if precipitation had occurred. Moreover, the Debye temperature for this sample is consistent with other measurements for fully dissolved Sn-Pb alloys.

The second measurement was the value of the line shift. The isomer shift of tin in tin is 2.5 mm/s at room temperature[20] while the measured value is 2.0 mm/s for the AgSn alloys, and 3.1 mm/s for the PbSn alloys, all relative to calcium stannate. The temperature dependence of the isomer shift in our samples is as expected from relativistic effects. This isomer shift is in disagreement with tin precipitates of appreciable size.

The third measurement was the XAFS of the Sn K edge in dilute alloy samples of Sn in Pb. The XAFS at $T = 80$ K showed that the Sn was surrounded by only Pb near neighbor atoms for the 2% sample as expected by the phase diagram. Figure 7 shows the predicted XAFS, using FEFF theory,[21] of the isolated first neighbors if they are all Pb, all Sn, and 3 Sn and 9 Pb neighbors. It is estimated that the XAFS could detect Sn neighbors if they are 10% or more of the total. These three experiments rule out the possibility of precipitation as an explanation for the observed rapid drop at T_0 in the 1% Sn in Pb sample.

Although the Sn in Ag alloys are always in a range well below the solubility limits, a check of the reversibility of the temperature dependence of the Mössbauer spectra intensities was made for both the 2% and 4% Sn in Ag samples. No significant hysteresis was detected as shown in Fig. 3(a). Thus, we conclude that both for the 1% and 2% Sn in Pb samples and all of the Sn alloys in Ag, no precipitation is occurring in the temperature range where the $\ln I$ deviates from a linear T behavior.

Another suggested interpretation for our observations is that impurities at the grain boundaries dominate the measurements, and so what we see is not a bulk

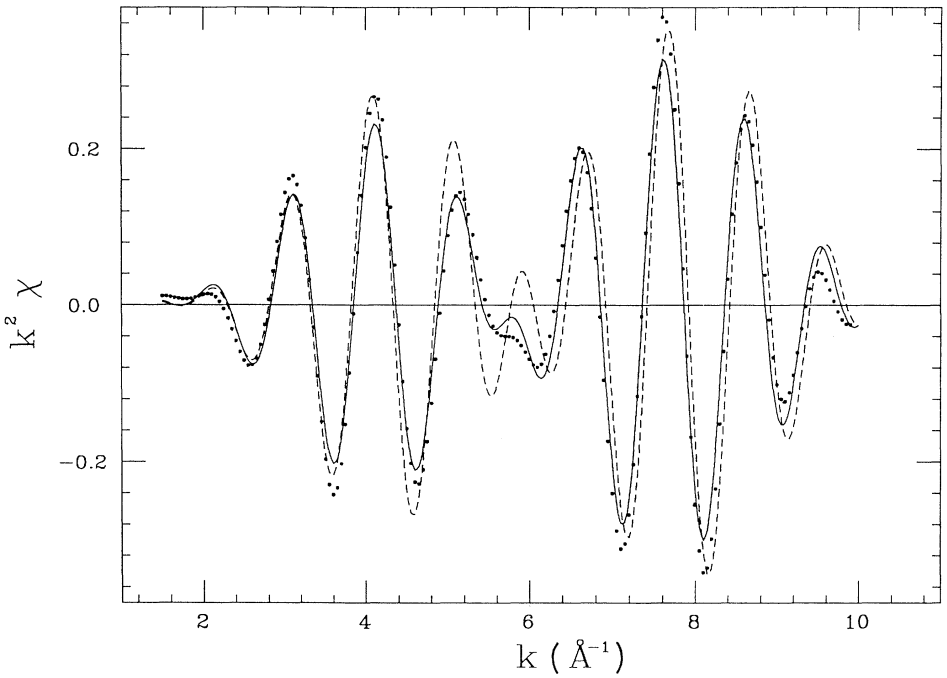

FIG. 7. The first shell XAFS of the K edge of Sn in an alloy of 2 at. % Sn in Pb is shown by dots. Calculations with 12 neighbors of Pb at 3.479 Å (solid), and with 9 Pb neighbors at 3.479 Å and 3 Sn neighbors at 3.479 Å (dash) are also shown. Note that the data are inconsistent with the latter model.

phenomenon but a "premelting" of the grain boundary. There is indeed an enhanced impurity concentration at the grain boundaries. For binary alloys with an impurity solubility limit on the order of 10%, the concentration of impurities at the grain boundaries is ~ 10 times greater than in the bulk.[22] The grain size of our samples is typically 1 μm. Since grain boundary widths are of the order of 10 Å, the fraction of the volume enclosed by grain boundaries is 0.001. Thus, only 1% of the impurities are in the grain boundaries, and the effect we observe must be a bulk phenomenon. In addition, the amount by which the grain boundary concentration is greater than the bulk concentration decreases with increasing temperature.[22] This too is contrary to the suggested interpretation that, as the sample is heated, the impurities move to the grain boundaries where "premelting" is more likely.

We now turn our discussion to the Pb host alloys. The 1% and 2% concentration samples clearly have no precipitates and the Sn is dissolved throughout the temperature range of the measurements. They show no irreversibility and are thus in thermal equilibrium. The very rapid decrease of the Mössbauer spectral intensity above T_0 is much too rapid to be explained by anharmonicity alone, and localized hopping of the atom off the lattice site must occur as discussed above. Also, as discussed in the experimental section, the 1% sample represents an isolated impurity. The temperature dependence of the Mössbauer spectral intensity below T_0 for the 1% sample is first fit to a σ_1^2 as in Eq. (2), giving the value of α, the temperature slope of $\ln I$, listed in Table I. Above T_0, the ratio between an extrapolation of this normal vibrational behavior and the observed anomalous drop in intensity gives from Eqs. (8) and (9b) the values of E and S presented in Table I. With the crude model of $n=2$ for the hopping state, this entropy translates to $L=43$ atoms involved in the hopping process. As another interpretation of this entropy, we compare it to the entropy of fusion S_f for Pb ($S_f \simeq 1.91$ e.u $\simeq 1.0 k_B$ per atom)[23] which allows for 30 atoms to have the same entropy as that in a liquid. To reiterate, the implication of $S=30k_B$ is that there are ~ 30 atoms around the Sn that are involved in a liquid-like hopping process with an entropy much higher than that of solid state diffusion. We call this region the high entropy or "premelted" bubble. It is much larger than the region over which the impurity itself moves.

A striking feature of Fig. 4(a) is the strong concentration dependence of the temperature dependence of the Mössbauer spectral intensity. The 2% sample has a smaller $|\alpha|$, a higher T_0 and a more gradual temperature variation than the 1% sample. Fitting the 2% data with Eqs. (8) and (9b) gives the values for α, E, S, and L in Table I.

The results of this analysis give an understanding of the concentration and temperature dependence found for the dilute Sn in Pb alloys. At low enough concentrations, the impurities have a premelted bubble of ~ 30 atoms surrounding them. This premelted bubble does not have the full disorder of a liquid since it is surrounded by crystalline Pb and the short-range order this induces orders the bubble substantially. It should be noted that a bubble of 30 atoms contains about 8 unit cubes or a radius of about one unit cube, i.e., about $1\frac{1}{2}$ nearest-neighbor distances. Short-range order in a liquid occurs over this same dimension and, therefore, will impose a strong constraint on the amount of disorder within the bubble. Yet, our experiments indicate that the Sn atom can still hop about within the bubble with the surrounding atoms participating in the motion.

When the concentration of the impurities becomes large enough to have substantial overlap of the bubbles

surrounding the impurities, they interact and, as the experiment indicates, the bubbles harden, i.e., the value of E increases, and their size increases, i.e., S increases. The hardening of the bubbles explains why the solid does not lose its rigidity as the concentration increases. The bubble surrounding the impurity explains why the interaction between impurities occurs at such low concentrations as 2%.

The behavior of the Ag based alloys is qualitatively somewhat different. The decrease below a linear behavior in Fig. 3(a) is initially much more gradual and at 900 K a more rapid drop occurs. Some concentration dependence is found. The most striking concentration dependence is exhibited by the line shift plots (Fig. 5). The 2% sample shows a linear T dependence and reversibility on heating and cooling. The 4% and 8% samples show a shift from the linear dependence at 500 K, and an irreversibility on an initial cycling. The concentration dependence suggests some interaction effect between the impurities is at the basis of the shift. We conclude that only the 2% Sn in Ag sample is an isolated impurity case.

The gradual decrease of $\ln I$ in Fig. 3(a) from a linear behavior is not anomalous and can be fit by anharmonicity as given in Eq. (2). The coefficients of the terms linear and quadratic in T in σ^2 are listed in Table I. The quadratic term is the anharmonic term and its magnitude is reasonable compared to the linear harmonic term, e.g., at 1000 K, near the melting temperature, the two terms are comparable. However, the more rapid drop at $T_0=900$ K requires the hopping mechanism. Fits to these drops using Eqs. (9b) and (8) for 2% and 4% Sn in Ag result in the values listed in Table I. The values of L are obtained from $S_f \sim 2.2$ e.u. for Ag.[23] The concentration dependence in E and S is similar to that in the Pb host indicating a similar hardening and growth in bubble size with increasing concentration.

However, the behavior of the two alloy based systems is different in some respects. The rapid decrease in the spectral intensity occurs at a much lower temperature for the Pb based alloys than the Ag based ones. This is true even if the data are normalized to the different melting temperatures of the host materials. One possible explanation of this difference is the difference of the relative sizes of the host atoms to the Sn atoms. The metallic radii of Ag, Pb, and Sn are 1.44, 1.75, and 1.40 Å, respectively. Tin impurities contract[24] the lattice constant of Pb but expand[25] that of Ag. Thus Sn has much more encapsulated space in a Pb host than it does in a Ag host. This large excess free volume available for Sn in Pb should greatly expediate a liquidlike hopping behavior. However, it should be noted that one should not treat the atoms as hard spheres with a fixed atomic radius. The XAFS measurement of 2% Sn in Pb, shown in Fig. 7, indicates that the Sn-Pb distance is 3.479 Å, only slightly smaller than the average interatomic distance of 3.498 Å found by x-ray diffraction, and considerably larger than the sum of the metallic radii of Sn and Pb (which gives 3.15 Å).

One can obtain an appreciation of how enhanced the local motion of the impurity is by comparing to the solid bulk diffusion rate. The extrapolated value of the solid bulk diffusion rate[26] of Sn in Pb at 150 K is 4×10^{-35} cm^2/s and it would take 10^{19} seconds to diffuse 3.5 Å, an atomic spacing. The local hopping is occurring in less than the Mössbauer lifetime ($\sim10^{-7}$ s), about 26 orders of magnitude more rapid. For the Ag host, the corresponding numbers at 900 K are[27] 8×10^{-11} cm^2/s, and 10^{-7} s to diffuse 2.9 Å. Here the bulk diffusion is comparable to the local hopping rate, but the sudden drop in the spectral intensity cannot be explained by bulk diffusion because there is no increase in line width. A more careful estimate from Singwi and Sjölander taking into account the discrete hopping motion shows that the line broadening is given by $\Delta_{\text{bulk}} \approx 12D\hbar/l^2$, where $l \approx 2.9$ Å. This gives a contribution of only 2% to the measured linewidth. Thus, bulk diffusion only slightly broadens the linewidth within experimental uncertainties, but does not decrease its intensity.

In an interesting paper Martin and Singer (MS)[9] investigated the behavior of point defects in a model crystal near melting by computer simulation. They misinterpreted our concept of a "premelted" bubble and assumed an actual bulklike liquid within the bubble without any short-range correlation with the surrounding solid. Their simulations could not sustain any such liquid bubble below T_m and wrongly concluded that their simulations were in disagreement with our model. It is clear why a bulklike liquid cannot be maintained below T_m in a bubble of diameter only a few atom spacings. The bubble, in contact with the surrounding solid, will have imposed on it short-range order as discussed above. This short-range order, even in a bulklike liquid, is not too different from a solid within an atom spacing or so. Thus, such a small bubble will not appear much more disordered than a solid. Its main feature is its ability to have correlated movements of the enclosed atoms to allow the impurity to move about its original site by more than 0.2 Å. This motion is different than hopping in a solid because it is a higher entropy process, more like a flow than a hopping.

Martin and Singer discovered the formation of interstitial-vacancy (IV) pairs for an impurity with a substantially smaller radius than the host at temperatures well below melting. Their IV pairs cannot explain our results because the interstitial in their case unbinds easily and contributes to the bulk diffusion rate, causing it to increase noticeably—an effect not seen. They speculate that there may be some lower temperature where the IV formation is frequent, but the interstitial and vacancy remain closely bound to each other and eventually recombine.

Our excited state is a bound IV pair in the MS terminology. The motion of the atom off the original lattice site produces a vacancy there and the atom, being off a lattice site, is in an interstitial position. However it is different in two important respects. One, the motion is not a hopping process as in a solid but a higher entropy one where the surrounding atoms participate more by flowing as in a liquid. Two, it is unlikely that the displacement of the pair is as large as in a classical interstitial of the FCC structure of Ag and Pb. It is hard to understand how such a well-separated IV pair (2.47 Å for octahedral and 2.14 Å for tetrahedral interstitial sites in Pb) can remain so tightly bound as required by our exper-

iment. For example, such IV pairs have been suggested[26] as a mechanism for the diffusion of Hg in Pb. In that case the various correlation coefficients are calculated to be greater than 0.25 above 500 K, e.g., the IV pair will move in less than four hops of the impurity. If this were the mechanism for the rapid local motion of Hg impurities in Pb seen[6] by XAFS, the bulk diffusion rate would be close to the liquid value, i.e., many orders of magnitude larger than the true value. Our experiment requires that the IV separation be greater than 0.2 Å, but the strong localization of the IV pairs that corresponds to localized motion in our model argues that the separation be significantly less than 2 Å. It should be emphasized that in addition to the motion of the impurity we find a high entropy bubble that contains ~ 30 surrounding atoms, and is thus about 5 Å in radius.

Tin is not an anomalous diffusor in Pb (Ref. 26) nor in Ag (Ref. 27). Its diffusivity in those hosts is similar in value to that of the self-diffusion of the hosts themselves. The mechanism usually postulated for such normal diffusion is a vacancy one.[26] With such a mechanism the diffusion rates of the host and impurity are within an order of magnitude of one another. Anomalous diffusors are impurities which have diffusion rates many orders of magnitude more rapid than the host. The mechanism for this anomalous diffusion is not known but it is usually associated with those impurities that dissolve as interstitials[26] and not substitutionally as Sn does in Pb and Ag.

An unusual local hopping phenomena was found[28] for Co impurities in Al. The Al interstitials were produced by low-temperature irradiation with high-energy electrons. Mössbauer spectroscopy on the ^{57}Co impurities indicated a rapid decrease in the recoiless fraction by more than a factor of 4 in the temperature interval between 13 and 20 K. This unusual behavior was attributed to the Co atom being itself in an interstitial site as it formed a dumbbell defect with an Al interstitial across the face of the unit cell cube. It was postulated that the Co interstitial hopped between the six equivalent sites corresponding to forming dumbbell defects across each face of the unit itself. This hopping was thermally activated in a temperature interval 13–20 K to cause the rapid drop in the recoiless fraction. Such a model cannot fit our situation as our samples are well annealed and we do not expect any significant number of self-interstitials to exist. The phase diagrams for Pb-Sn and Ag-Sn as verified by diffraction and by XAFS for Pb-Sn indicate that Sn is a substitutional impurity, not an interstitial one.

There have been attempts to detect "premelting" phenomena in solids with the motive to detect an instability in the solid which causes the melting transition. The classical thermodynamical picture of melting is that it is not caused by an instability, but it is a first-order phase transition wherein the liquid phase becomes thermodynamically more stable. The solid is still mechanically stable and the transition to the liquid phase is a nucleation and growth process. Molecular-dynamic simulations[1] confirm the thermodynamic picture. Our "premelting bubbles" are not an instability of the solid but an equilibrium state. There is no reason to expect the solid to be completely homogeneous on an atomic scale when it has impurities to destroy the periodicity.

The mechanism of melting therefore requires specifying the nucleation site where the growth initiates. For small samples where the surface or interface is not negligible, nucleation can initiate on these surfaces.[1–4] These interfaces show "premelting" disorder below the melting temperature and they subsequently act as the nucleation sites at melting. However, in large single crystals (rigorously, when the volume goes to infinity) where the surface and grain boundary areas can be neglected, the initiation sites must scale with the volume. The regions surrounding those impurities which exhibit the "premelted" bubbles do scale correctly and will have a smaller barrier to a fluctuation to a nucleation site and could serve as the initiation sites for melting in 3D in the thermodynamic limit of very large single crystals, analogous to the "premelted" interfaces for smaller crystals. Impurities are only one type of a possible whole class of point defects which could act as initiation sites for 3D melting. Any point defect that increases the free volume for hopping such as vacancies may also show "premelting" in its vicinity and thus act as an initiation site. Since vacancies are thermally excited in all solids, this could be a mechanism for melting even in pure materials. It is pertinent to mention here that very recent molecular-dynamics calculations of Car[29] near the melting point of Si show such "premelting" characteristics around vacancies. Whereas at low temperatures the diffusion in the vicinity of the vacancy consists of a single atom hopping, near the melting point a significant fraction of the diffusion processes consists of several atoms moving coherently, i.e., a high entropy type flow as in a liquid.

The temperature dependence of the spectral intensities that we measure are consistent with other measurements. In unpublished thesis work,[30] Knauer found a temperature dependence similar to ours for the spectral intensity of Sn in Ag, but measured up to only 743 K, and so did not see the temperature range with the rapid drop. Room-temperature values for the recoilless fraction of dilute Sn impurities in Pb have been measured[31] to be 0.016 (0.015). Finally, it should be noted that possible premelting of the Ag^+ ionic sublattice surrounding impurity Sn atoms has been reported[32] in a Mössbauer experiment on superionic Ag_2Se with tin impurities.

IV. SUMMARY AND CONCLUSIONS

When the periodicity of Pb and Ag is disrupted by the addition of Sn impurities the homogeneity of behavior on the atomic scale is also disrupted. Isolated Sn impurities, which lower the melting temperature T_m of both hosts, exhibit an anomalously rapid localized motion at temperatures well below bulk melting. This motion has the characteristics of a liquidlike local diffusion because of the high entropy associated with it. It is estimated that about 30 atoms are associated with the anomalous motion in Pb and somewhat more in Ag. These atoms constitute a region around the impurity with higher entropy density than the rest of the solid. The temperature where the anomalous localized motion becomes appreciа-

ble during the 10^{-7} s of the Sn Mössbauer lifetime is about $\frac{1}{4}T_m$ for the Pb host and about $\frac{3}{4}T_m$ for the Ag host. This difference in temperatures is correlated with the "free volume" surrounding the impurity. Sn contracts the Pb lattice while it expands the Ag lattice, indicating that it has more encapsulated space in Pb than in Ag. It is argued that the high entropy density regions surrounding the Sn impurities can act as nucleation sites for three-dimensional melting in competition with grain boundaries and surfaces. For large enough samples the impurity sites will dominate. It is suggested that other point defects can also act as nucleation sites for three dimensional melting. In particular, thermally excited vacancies may be nucleation sites for bulk melting of pure materials.

ACKNOWLEDGMENTS

Valuable discussions are gratefully acknowledged with John W. Cahn, J. G. Dash, and Yu. Khait. Research supported by Technion V.P.R. fund, S. Langberg Nuclear Research Fund, BSF 88-00240, and DOE Grant No. DE-FG06-90ER45425.

APPENDIX

We now derive Eq. (3) for the Mössbauer spectrum of a system with the absorbing atom having two possible states, one vibrating about the lattice site, and the other hopping around the lattice site. We take P to be the probability of being in the vibrating state (state 1) with distribution around the lattice site $\rho_1(\mathbf{r})$. The hopping state (state 2) has probability $(1-P)$ and distribution $\rho_2(\mathbf{r})$. The origin is chosen at the lattice site.

The Mössbauer spectrum is given by[15]

$$W(q,\omega)=\int d\mathbf{r}\,dt\,\exp[i(\mathbf{q}\cdot\mathbf{r}-\omega t)-(\Gamma/2\hbar)|t|]G_s(\mathbf{r},t)\ , \tag{A1}$$

where Γ is the Mössbauer line width, and

$$G_s(\mathbf{r},t)=\left\langle\int d\mathbf{r}'\delta(\mathbf{r}+\mathbf{r}'-\mathbf{R}(t))\delta(\mathbf{r}'-\mathbf{R}(0))\right\rangle_T \tag{A2}$$

is the correlation between the position of the same Mössbauer particle at different times.

In evaluating $G_s(\mathbf{r},t)$, we are interested in those times that may affect the Mössbauer line shape. We assume that τ_0, the time to equilibrate within a given state, is much smaller than both $\tau_M=(\hbar/\Gamma)$ and $\tau_{\rm eq}=(\hbar/\Delta)$, where τ_M is the Mössbauer lifetime, and $\tau_{\rm eq}$ is the time scale for the two states to reach equilibrium. We show below that a particle starting in either of the two states approaches equilibrium at the same rate. The time τ_0 is on the order of a vibrational period, and so is clearly much less than τ_M, and will therefore contribute only a broad background to the Mössbauer spectrum. For this reason we only need to consider times $t\gg\tau_0$ in evaluating $G_s(\mathbf{r},t)$. For such times, $G_s(\mathbf{r},t)$ is dependent on the initial state in which the atom is distributed, but is independent of the initial position $\mathbf{R}(0)$ of the Mössbauer atom. The average can therefore be done first over the initial position $\mathbf{R}(0)$, and then done over $\mathbf{R}(t)$ where care must be taken to consider the initial state of the particle. The first average gives

$$\langle\delta[\mathbf{r}'-\mathbf{R}(0)]\rangle_T=P\rho_1(\mathbf{r}')+(1-P)\rho_2(\mathbf{r}')\ , \tag{A3}$$

which gives the equilibrium distribution of the initial state. We are left with

$$G_s(\mathbf{r},t)=PG_1(\mathbf{r},t)+(1-P)G_2(\mathbf{r},t)\ , \tag{A4}$$

where

$$G_i(\mathbf{r},t)=\int d\mathbf{r}'\rho_i(\mathbf{r}')\langle\delta(\mathbf{r}+\mathbf{r}'-\mathbf{R}(t))\rangle_{i,T},\quad i=1,2\ , \tag{A5}$$

and the average is now only over $\mathbf{R}(t)$ for each of the two possible initial states.

These two averages are

$$\begin{aligned}\langle\delta(\mathbf{r}+\mathbf{r}'-\mathbf{R}(t))\rangle_{1,T}&=\rho_1(\mathbf{r}+\mathbf{r}')[P+(1-P)e^{-(\Delta/\hbar)t}]\\&\quad+\rho_2(\mathbf{r}+\mathbf{r}')[(1-P)(1-e^{-(\Delta/\hbar)t})]\end{aligned} \tag{A6}$$

and

$$\begin{aligned}\langle\delta(\mathbf{r}+\mathbf{r}'-\mathbf{R}(t))\rangle_{2,T}&=\rho_2(\mathbf{r}+\mathbf{r}')[(1-P)+Pe^{-(\Delta/\hbar)t}]\\&\quad+\rho_1(\mathbf{r}+\mathbf{r}')[P(1-e^{-(\Delta/\hbar)t})]\ ,\end{aligned} \tag{A7}$$

both of which can easily be verified to give the correct results for $t=0$ and $t\gg(\hbar/\Delta)$. [The result for $\langle\delta(\mathbf{r}+\mathbf{r}'-\mathbf{R}(0))\rangle_{i,T}$ is $\rho_i(\mathbf{r}+\mathbf{r}')$. At long times, the equilibrium expression of Eq. (A3) is recovered.] Combining all these gives

$$\begin{aligned}G_s(\mathbf{r},t)=\int d\mathbf{r}'\{&\rho_1(\mathbf{r}')\rho_1(\mathbf{r}+\mathbf{r}')[P^2+P(1-P)e^{-(\Delta/\hbar)t}]+P(1-P)[\rho_1(\mathbf{r}')\rho_2(\mathbf{r}+\mathbf{r}')+\rho_2(\mathbf{r}')\rho_1(\mathbf{r}+\mathbf{r}')](1-e^{-(\Delta/\hbar)/t})\\&+\rho_2(\mathbf{r}')\rho_2(\mathbf{r}+\mathbf{r}')[(1-P)^2+P(1-P)e^{-(\Delta/\hbar)t}]\}\ .\end{aligned} \tag{A8}$$

Taking the Fourier transform, as in Eq. (A1), we get

$$\begin{aligned}W(q,\omega)=&P^2\rho_1^2(\mathbf{q})\mathcal{L}(\Gamma,\omega)+P(1-P)\rho_1^2(\mathbf{q})\mathcal{L}(\Gamma+\Delta,\omega)+2P(1-P)\rho_1(\mathbf{q})\rho_2(\mathbf{q})[\mathcal{L}(\Gamma,\omega)-\mathcal{L}(\Gamma+\Delta,\omega)]\\&+(1-P)^2\rho_2^2(\mathbf{q})\mathcal{L}(\Gamma,\omega)+P(1-P)\rho_2^2(\mathbf{q})\mathcal{L}(\Gamma+\Delta,\omega)\ ,\end{aligned} \tag{A9}$$

where $\mathcal{L}(\Gamma,\omega)$ is the usual Lorentzian defined in Eq. (4), and $\rho_i(\mathbf{q})$ is the Fourier transform of $\rho_i(\mathbf{r})$. For $\rho_i(\mathbf{r})$ that are Gaussian distributions with mean-square disorder σ_i^2, Eq. (A9) reduces to Eq. (3).

The rate Δ is related to the relaxation of states 1 and 2 by the relations

$$\frac{dN_1}{dt} = -N_1\Delta_1 + N_2\Delta_2 , \tag{A10}$$

$$\frac{dN_2}{dt} = N_1\Delta_1 - N_2\Delta_2 , \tag{A11}$$

where N_i are the numbers of particles in state i and Δ_i are the relaxation rates of each state. For equilibrium values of N_i, there is no time dependence and

$$N_1^0\Delta_1 = N_2^0\Delta_2 . \tag{A12}$$

In terms of N_i^0, we have

$$P = \frac{N_1^0}{N_1^0 + N_2^0} ,$$

so that

$$P\Delta_1 = (1-P)\Delta_2 . \tag{A13}$$

For a deviation from equilibrium, $\delta N = N_1 - N_1^0 = -(N_2 - N_2^0)$, Eqs. (A10) and (A11) give

$$\frac{d\delta N}{dt} = -\Delta\,\delta N , \tag{A14}$$

where

$$\Delta = (\Delta_1 + \Delta_2) = \Delta_1\left[\frac{1}{1-P}\right] = \frac{\Delta_2}{P} . \tag{A15}$$

We note that $\Delta \gg \Delta_1$ for $P \approx 1$, which can explain why at T_0 there is no noticeable broadening component starting to appear as the transition to state 2 begins. Although at T_0 one may expect Δ_1 to be initially small, Δ will be much larger and could then be buried in the background, consistent with the measurements.

[1] S. R. Phillpot, S. Yip, and D. Wolf, Comput. Phys. **3**, 20 (1989).
[2] M. E. Glicksman and C. E. Vold, Surf. Sci. **31**, 50 (1972).
[3] R. K. Kuchi and J. W. Cahn, Phys. Rev. B **21**, 1893 (1980); **36**, 418 (1987).
[4] T. Nguyen, P. S. Ho, T. Kwok, C. Nitta, and S. Yip, Phys. Rev. Lett. **57**, 1919 (1986).
[5] H. Schechter, E. A. Stern, Y. Yacoby, R. Brener, and Z. Zhang, Phys. Rev. Lett. **63**, 1400 (1989).
[6] E. A. Stern and K. Zhang, Phys. Rev. Lett. **60**, 1872 (1988).
[7] E. A. Stern, P. Livins, and Z. Zhang, Phys. Rev. B **43**, 8850 (1991).
[8] J. Mullen (private communication).
[9] C. H. Martin and S. J. Singer, Phys. Rev. B **44**, 477 (1991).
[10] J. D. Donaldson, R. Oteng, and B. J. Senior, Chem. Commun. **24**, 618 (1965).
[11] See, e.g., S. S. Hanna and R. S. Preston, Phys. Rev. **139A**, 722 (1965); Goldanski and R. H. Herber, in *Chemical Applications by the Mössbauer Spectroscopy* (Academic, New York, 1968).
[12] W. Kohn and S. H. Voski, Phys. Rev. **119**, 912 (1960).
[13] H. Frauenfelder, *The Mössbauer Effect* (Benjamin, New York, 1962), p. 45.
[14] See, e.g., S. Margulies and J. R. Ehrman, Nucl. Instrum. Methods **12**, 131 (1961).
[15] K. S. Singwi and A. Sjolander, Phys. Rev. **120**, 1093 (1960).
[16] P. D. Mannheim, Phys. Rev. **165**, 1011 (1965); P. D. Mannheim and A. Simopolous, *ibid.* **165**, 845 (1965); P. D. Mannheim and S. S. Cohen, Phys. Rev. B **4**, 3748 (1971); P. D. Mannheim, *ibid.* **5**, 745 (1972).
[17] D. G. Howard and R. H. Nussbaum, Phys. Rev. B **9**, 794 (1974).
[18] M. Hansen, *Constitution of Binary Alloys* (McGraw-Hill, New York, 1958), p. 1107.
[19] H. Arriola and T. E. Cranshaw, J. Phys. F **18**, 1621 (1988).
[20] J. K. Lees and P. A. Flinn, J. Chem. Phys. **48**, 882 (1968).
[21] J. J. Rehr, R. C. Albers, and S. I. Zabinsky, Phys. Rev. Lett. **69**, 3397 (1992); J. J. Rehr and R. C. Albers, Phys. Rev. B **41**, 8139 (1990).
[22] E. D. Hondros and M. P. Seah, Int. Metall. Rev. **222**, 263 (1977).
[23] A. R. Ubbelhode, *The Molten State of Matter* (Wiley, New York, 1978), p. 239.
[24] W. B. Pearson, *Handbook of Lattice Spacings and Structure of Metals and Alloys* (Pergamon, Oxford, 1958), p. 807.
[25] W. B. Pearson, *Handbook of Lattice Spacings and Structure of Metals and Alloys* (Ref. 23), p. 304.
[26] W. K. Warburton and D. Turnbull, in *Diffusion in Solids,* edited by A. S. Nowick and J. J. Burton (Academic, New York, 1975), Chap. 4.
[27] C. T. Tomizuka and L. Slifkin, Phys. Rev. **96**, 610 (1954).
[28] G. Vogl, W. Mansel, and P. H. Dederichs, Phys. Rev. Lett. **36**, 1497 (1976).
[29] R. Car (private communication).
[30] R. C. Knauer, Jr., Ph. D. thesis, Purdue University, 1969.
[31] H. Andreasen, S. Damgaard, J. W. Petersen, and G. Weyer, J. Phys. F **13**, 2077 (1983).
[32] M. Pasternak, N. Benczer-Koller, T. Yang, and R. H. Herberg, Phys. Rev. B **27**, 2055 (1983).